VORTICITY-TRANSPORT AND UNSTRUCTURED RANS INVESTIGATION OF ROTOR-FUSELAGE INTERACTIONS

Marilyn J. Smith
Associate Professor

Rajiv Shenoy
Graduate Research Assistant

Daniel Guggenheim School of Aerospace Engineering
Georgia Institute of Technology, Atlanta, GA 30332-0150, USA

Adam R. Kenyon
CFD Engineer
Red Bull Racing
Milton Keynes, UK

Richard E. Brown
Mechan Chair of Engineering
University of Glasgow
Glasgow, UK

Abstract

The prediction capabilities of unstructured primitive-variable and vorticity-transport-based Navier-Stokes solvers have been compared for rotorcraft-fuselage interaction. Their accuracies have been assessed using the NASA-Langley ROBIN series of experiments. Correlation of steady pressure on the isolated fuselage delineates the differences between the viscous and inviscid solvers. The influence of the individual blade passage, model supports, and viscous effects on the unsteady pressure loading has been studied. Smoke visualization from the ROBIN experiment has been used to determine the ability of the codes to predict the wake geometry. The two computational methods are observed to provide similar results within the context of their physical assumptions and simplifications in the test configuration.

1. NOMENCLATURE

c	rotor blade chord length, inches
C_p	pressure coefficient $\frac{p-p_\infty}{0.5\rho U_\infty^2}$
$C_{p'}$	modified pressure coefficient $\frac{p-p_\infty}{0.5\rho(\Omega R)^2} \times 100$
c_T	thrust coefficient
l	fuselage half-length, inches
M	Mach number
r	rotor radial location, inches
R	rotor tip radius, inches
Re	Reynolds number
S	source term
x, y, z	Cartesian streamwise,radial and normal lengths, inches
$\mathbf{u}$	local velocity, $\frac{ft}{sec}$
U_∞	free stream velocity, $\frac{ft}{sec}$
α_s	shaft tilt (positive aft), deg
β_0	coning angle, deg
ω	vorticity
Ω	rotor speed, rpm
ψ	blade azimuth angle, deg
σ	rotor solidity
μ	advance ratio, $\frac{U}{\Omega R}$
θ_0	collective angle, deg
θ_{1c}	lateral cyclic angle, deg
θ_{1s}	longitudinal cyclic angle, deg

2. BACKGROUND

The interaction of the rotor wake with the helicopter fuselage or empennage can affect vehicle performance, acoustic signature and structural response. Time-averaged loading on the fuselage will dictate vehicle performance, while shed vorticity impinging on the empennage can result in buffet, causing increased component fatigue and failure. Vortex passage near or impact on the fuselage surface will influence noise (aero and structural) characteristics and handling qualities as the surface pressures fluctuate during each rotor revolution.

Computational methodologies for rotorcraft applications have undergone significant development in the past two decades as the performance of computer hardware has

logarithmically increased while the cost per processor has similarly decreased. Today's computers have the capability to resolve the Navier-Stokes equations for complex time-accurate applications, permitting solutions that capture more of the flow field physics. Strawn[1] has compiled a history of Computational Fluid Dynamics (CFD) advancements for rotorcraft through the first half of the current decade, illustrating the development of computational methodologies from potential solvers coupled with vortex element models to multi-topology overset formulations of the Navier-Stokes equations. While rotors are well suited to grid meshing by structured-grid-based Reynolds-averaged Navier-Stokes (RANS) CFD methods, the flow field solution can suffer from high dissipation unless the wake region is modeled via a refined mesh, resulting in high computational costs. As noted in the study by Strawn and Djomehri[2] of a UH-60A rotor in hover, the computational solution experienced a persistent grid dependence, and even with a 64 million node structured grid, the numerical dissipation of vorticity still overwhelmed the physical behavior of their system. The rotor in this simulation was modeled by embedded momentum sources to minimize the computational grid size.

Computational simulation of rotor-fuselage interaction (RFI) strains even further the resources required by structured methods. At minimum, unsteady source modeling of the rotor is required to obtain an estimate of the unsteady fuselage surface pressures,[3] and the exact representation of the moving rotor blades is requred to accurately evaluate the unsteady wake and its interaction with other components such as the fuselage, empennage or external structures. In addition, the helicopter configuration is complex and requires the use of a large number of overset structured meshes to model abrupt changes in the geometry. Potsdam and Strawn[4] studied a full-span V-22 configuration with moving rotor blades. Their structured overset RANS solver required a significant number of overset grids totaling 47.6 million nodes.

There are several alternate routes to permit more flexibility in the placement of the computational nodes and to reduce the complexity of the grid generation process that is required as a pre-requisite for the simulation of the aerodynamics of modern helicopter configurations. Researchers using conventional RANS-based CFD methods in RFI have developed and applied alternative computational grid topologies, including unstructured,[5] Cartesian[6] or a combination of several grid topologies.[7] Cartesian methods do not require body-fitted grids, and thus most of the time-consuming grid generation activity is not necessary. Problems still exist in modeling rapid geometry changes and viscous simulations about complex geometries due to the nature of the boundary conditions. Unstructured RANS methods use either a fully tetrahedral grid topology or a mix of prisms, tetrahedral and hexahedral cells to compose the grid. This approach permits complex geometries to be modeled much more rapidly than is the case with their structured method counterparts, and a single grid surrounding the fuselage can be extended efficiently to form the background or far-field grid. Unstructured methods are not without their problems, as current solvers cannot efficiently obtain high-order spatial resolution (e.g., 4th or 6th order), and their computational overhead and cost per iteration are significantly higher than with structured methods.

Because RFI consists of two frames of motion to capture the moving blades and nonrotating fuselage, various techniques to include both frames of motion have been explored. Lee and Kwon[8] and Steijl and Barakos[9] have both demonstrated variations of sliding boundary conditions between rotor and fuselage grids. Other researchers[3,5,6,10] have applied overset methods to resolve the disparate frames for RFI. While the sliding boundary methods have some advantage in reducing grid points as overlap grids are not needed, the overset methods have greater flexibility to permit modeling of counter-rotating rotors and aeroelastic (CFD/CSD) motions. Overset methods also allow configuration changes to be modeled with relative ease as individual grids containing components such as hubs, rotors, and struts can be added (or removed) from the computational model with little difficulty. Grid adaptation and higher-order methods are also options that can be exploited to improve accuracy while reducing the size of the flow field grid. An overview of the capability of these methods to capture wake vorticity can be found in Komerath and Smith.[11]

Hybrid techniques model the near-field of the rotor and fuselage using computational methods designed for accuracy near surfaces, while the wakes are resolved via methods that are known to propagate the wake vorticity without dissipation at a relatively low cost. Conventional hybrid methods employ either panel or CFD RANS techniques for regions near the rotorcraft and resolve the wake using a potential method based typically on a Lagrangian prescribed or free wake technique. While the structure of the wake is efficiently resolved by the potential method, thus obviating the need for large quantities of grid nodes, these methods rely on empirical models to describe the behavior of the vortex-dominated wake. In addition, the boundary conditions that are required at the interface between the two methods may have difficultly in maintaining the resolution of vortices that reenter the RANS grids.

An alternative approach which has shown signficant promise in addressing the dissipation and the cost of

traditional CFD techniques in the wake, while capturing the behavior of the vortex core and shed wake that must be modeled with potential-based Lagrangian techniques is the vorticity transport method (VTM). VTM resolves the Navier-Stokes equations in vorticity-velocity form, rather than the traditional primitive (i.e., pressure-velocity-density) form solved by RANS CFD methods. By casting the vorticity within the flow as the primary conserved variable, the dissipation of vortical structures that is a common feature of primitive variable CFD solvers is avoided entirely. Indeed, the effects of numerical diffusion on the integrity of vortical structures within the flow can be controlled very effectively by suitable choice of the numerical algorithm that is used to advect the vorticity through the computational domain. One of the most successful of such approaches is the vorticity transport model (VTM), developed by Brown[12] and extended by Brown and Line.[13] This model has been exploited extensively within the rotorcraft field, where it has been applied to helicopter flight mechanics research by Brown and Houston[14] and Houston and Brown,[15] for the investigation of the interaction of helicopters with aircraft wakes by Whitehouse and Brown,[16] the rotor vortex ring state by Ahlin and Brown,[17] and rotor-induced brownout by Phillips and Brown.[18]

The principal impediment to consistent use of the vorticity transport approach throughout the flow field is the difficulty in applying consistent and physically-rigorous boundary conditions on solid surfaces immersed within the flow. This is mitigated to some extent by the ability of the formulation to accommodate a wide range sources of vorticity in the flow, from lifting-line type comprehensive rotor models through to hybridizations with existing primitive-variable CFD type approaches. As such VTM has been used with considerable success to resolve the close wake-body interactions of the ROBIN system,[19] rotor blade-vortex interactions,[20] main rotor-tail rotor interactions,[21] and the complex inter-rotor interactions of advanced rotorcraft configurations such as the thrust-compounded coaxial helicopter.[22]

While both these numerical methods have been correlated independently with experimental data, no formal comparison of their predictive abilities has as yet been accomplished for a vortex-dominated rotorcraft application. Such a comparison is warranted as the research and engineering rotorcraft community must develop and apply discriminators when selecting appropriate computational methods for complex configurations. To wit, this paper compares an unstructured RANS CFD method, FUN3D, and the VTM method for the rotor-fuselage interaction problem. Their behavior in capturing the unsteady pressure effects on the fuselage is studied, noting the accuracy of each method, as well as detailing the nuances of each method's abilities. The methods' abilities to capture the wake structure for the rotor-fuselage interaction is likewise compared. This study does not seek to select the "best" method, but provides information to the engineering community so that the most appropriate method to capture particular features of a problem can be determined.

3. EXPERIMENTAL DATASET FOR CORRELATION

Investigations into the nature of rotor airframe interactions were conducted on the ROtor Body INteraction (ROBIN) model by several researchers at NASA Langley Research Center. The ROBIN model can be constructed from a set of algebraic equations at various fuselage stations to yield a streamlined slender fuselage body with little separation at low angles of attack. An engine mount, or "doghouse", is included in the configuration. Freeman and Mineck[23] studied the steady pressures on the ROBIN fuselage without the rotor. These are useful to determine the fidelity of the grid necessary to model the fuselage prior to the addition of the rotor blades.

Subsequent ROBIN studies added a 4-bladed rotor with 0.098 solidity. Each rotor blade was a rectangular planform with a NACA0012 airfoil section and -8° linear twist from root to tip. The rotor blade chord was 2.7 inches, while the radius was 33.88 inches with a 24% root cutout. Mineck and Althoff-Gorton[24] extended the ROBIN study to include measurements of the unsteady pressures on the surface of the fuselage. This last data set documents the influence of the rotor wake and blade passage on the surface pressures over a range of advance ratios. Several of the Mineck and Althoff-Gorton experimental cases are studied in this work, as listed in Table 1. For these tests, the rotor was mounted on a separate sting extending down from the ceiling, and the hub was mounted at (0.697, 0.051, 0.322) in normalized dimensions (with respect to the fuselage half-length, 39.35 inches). The fuselage was run at 1.2° yaw angle for all test cases in Table 1. Unsteady pressure data for the fuselage was time-averaged over thirty rotor revolutions, although for some test conditions, 40% variation in magnitude at some fuselage centerline locations was still reported. In this study, the unsteady pressure data have been shifted by a phase of 252°[25] to compensate for phase lags in the experiment.

Table 1: Unsteady Pressure Experimental Test Cases. From Mineck and Althoff-Gorton (Ref. 24)

μ	C_T	α_s (◦)	θ_0 (◦)	θ_{1c} (◦)	θ_{1s} (◦)
0.05	0.0064	0.0	11.9	-1.3	1.3
0.15	0.0064	-3.0	10.3	-2.7	2.4
0.23	0.0040	-3.0	8.2	-0.5	3.8
0.23	0.0064	-3.0	10.4	-0.4	3.8
0.23	0.0080	-3.0	11.9	-1.3	4.0

Ghee and Elliott[26] studied the wake geometry, which including tighter vortex rollup on the rotor advancing side compared with the rotor retreating side. Smoke visualization was used to capture the vortex trajectories. This experimental set-up varied from the unsteady pressure tests. The rotor was mounted internally, and the hub center was located at the half-fuselage-normalized coordinates, (0.697, 0.000, 0.275). The two test cases for the wake visualization, listed in Table 2, were run at a yaw angle of zero degrees.

Table 2: Wake Visualization Experimental Test Cases. From Ghee and Elliott.[26]

μ	C_T	α_s (◦)	β_0 (◦)	θ_0 (◦)	θ_{1c} (◦)	θ_{1s} (◦)
0.15	0.0064	-3.0	1.5	6.6	-1.4	2.0
0.23	0.0064	-3.0	1.5	6.5	-1.1	3.2

4. COMPUTATIONAL METHODOLOGIES

4.1. Vorticity-Transport Method

The VTM resolves the vorticity-velocity form

$$\frac{\partial}{\partial t}\omega + \mathbf{u}\cdot\nabla\omega - \omega\cdot\nabla\mathbf{u} = S + \nu\nabla^2\omega \tag{1}$$

of the Navier-Stokes equations on a Cartesian grid surrounding the rotorcraft. The velocity u is obtained from the vorticity field ω by inversion of the differential form of the Biot-Savart equation,

$$\nabla^2 u = -\nabla\times\omega \tag{2}$$

using a Cartesian Fast Multipole technique. The source term S in the current work is implemented using a lifting-line model for the trailed and shed vorticity into the computational domain.

Significant savings in memory and computational time are achieved by allowing the distribution of cells within the computational domain to track the vorticity field as it evolves. This is done by creating computational cells in regions of the flow where vorticity exists and subsequently destroying them once the vorticity migrates elsewhere. Computational efficiency is enhanced further by using a sequence of nested grids in which the cells within the outer grids are arranged to be coarser than those closer to the rotor. This reduces the overall cell count while allowing a highly resolved flow field to be maintained near the rotor. The convection algorithm implemented in the VTM is particularly effective in controlling the local rate of dissipation of the vorticity, allowing the integrity of vortical structures in the rotor wake to be preserved for many rotor revolutions. The VTM is thus particularly well suited to resolving the wake-induced interactions between geometrically well-separated components of the helicopter. In the context of the present paper, this property of the model enables the long-range aerodynamic interactions between the rotor and fuselage of the configuration under study to be captured in finer detail.

4.1.1. Rotor and Fuselage Grids

For the VTM results in this study, the blade aerodynamics were modeled using a variant of the Weissinger-L lifting-line theory. Aerodynamic sectional characteristics were provided as a table formatted as a function of local Mach number and angle of attack at each of 30 rotor radial stations for a prescribed Reynolds number. Profile drag estimates were computed by a separate computation based on the local angle of attack and added to the inviscid predictions.

The ROBIN fuselage was modeled via a vortex panel method, which forms a closed surface using quadrilateral panels. The panel system on the fuselage surface consisted of 2174 vortex panels. This grid was chosen to correlate with the change in the predicted rotor inflow; that is, additional panels resulted in only small changes in the rotor inflow predictions. This permitted the wake features to be modeled, while minimizing the computational requirements. No attempt was made to model the fuselage strut or the rotor hub that were present in the ROBIN experiments.

4.2. Unstructured RANS Method

The unstructured methodology chosen for this work is the NASA unstructured method, FUN3D. FUN3D implicitly resolves the primitive variable form of the Reynolds Averaged Navier-Stokes (RANS) equations using node-centered unstructured mixed topology grids.[27,28] Georgia Tech first successfully extended and utilized FUN3D for a number of applications in rotorcraft,[3,5,29] including rotor-fuselage interaction. Currently both Georgia Tech

and NASA Langley researchers[30,31] continue to expand FUN3D's capability with rotary-wing vehicles. FUN3D is capable of resolving both compressible and incompressible[32] Mach regimes. Time-accuracy is achieved via a 2^{nd}-order backward differentiation formula (BDF), while a point-implicit relaxation scheme is applied to the resulting linear system of equations. The Roe flux difference splitting technique[33] computes the inviscid fluxes, while viscous fluxes are resolved with an equivalent central difference approximation. Turbulence models available include both RANS Spalart-Allmaras[34] and Menter's kω-SST[35] models, as well as hybrid RANS-LES-based methods, including SA-DES[36] and GT-HRLES.[37]

4.2.1. Unstructured Computational Grid

For this study, NASA's VGRIDns[38] was used to generate a fully tetrahedral, overset mesh of the ROBIN fuselage, including an approximate sting similar to the rotor-fuselage ROBIN experiments. Views of the unstructured grid are shown in Fig. 1. The overset grid strategy allows mesh refinement near the fuselage and rotor blades, while minimizing the number of overset meshes. Each rotor blade is enclosed in a grid with a cylindrical near-body boundary aligned axially spanwise on the blade that extends 1 chord normal to the surface, and forward and aft of the blade. The cylinder ends are rounded such that the boundary extends 1chord beyond the tips. Grid independence studies were carried out for the fuselage-alone configuration, and the grid applied in this study showed little variation in surface pressures with more refined grids. Each near-body blade grid consisted of 2.3 million nodes (13.5 million cells) and the background grid, which included the fuselage, consisted of 5.1 million nodes (30.2 million cells). The outer boundary of the fuselage grid is five fuselage lengths from the surface, based on prior experience[3] with rotor-fuselage interaction problems using FUN3D.

4.2.2. Unstructured Numerical Simulations

The FUN3D solutions for this work were computed with the unsteady, compressible option. The solution was advanced with a time step equivalent to 1°. During each timestep, 15 sub-iterations were used to ensure 1-2 orders of magnitude residual reduction during each time step. Ten turbulence sub-iterations were also applied to converge the loosely-coupled Menter kω-SST turbulence model. The computations were performed on 64 2.3GHz processors of a CRAY XT5. The mean required CPU time is 2.97 msec/node/timestep, which includes the sub-iteration costs.

While the methodology does not include a trimming algorithm without CFD/CSD coupling, the thrust was trimmed interactively using the experimental thrust coefficient as the trim target value. After an initial periodic solution was determined, the thrust was assumed to vary linearly with collective. Collective estimates from the actual and target thrust values were applied as restarts to the existing solution with an equivalent time step of 3° until the solution was periodic, typically one revolution. Trim was achieved within 2 iterations, after which the solution was run for another revolution with a time step equivalent to 1° to ensure a periodic solution. All time steps included 15 sub-iterations and 10 turbulence sub-iterations.

5. RESULTS

5.1. Isolated Fuselage

The two computational methods utilized different levels of fidelity to model the fuselage, and the unstructured method also approximated the fuselage sting from the Mineck and Althoff-Gorton campaign.[24] To examine the influence that these differences in fuselage modeling may have on the results, comparisons were made with the experimental data of Freeman and Mineck[23] for the isolated fuselage. All results are shown here with the unstructured FUN3D grid used for subsequent computations as a grid refinement study showed only small changes in the pressures, primarily at the location of the fuselage strut.

Figure 2 locates the fuselage stations (x/l) where experimental pressure data around the fuselage radius (varying z/l) are available for correlation. FUN3D and VTM data correlate well with one another and with experimental data at these locations (Fig. 3). In instances where the two computational data are not coincident, they tend to bracket the experimental data with approximately the same difference. The largest differences are observed for the $x/l = 1.16$ location, which is just aft of the fuselage strut location. The VTM data indicate near-freestream pressure coefficients at the lower centerline (lowest z/l values) for the $x/l = 1.16$. The pressure coefficient becomes slightly more negative, implying that the flow has accelerated as the fuselage transitions to the side geometry. Flow velocity slows as the z/l increases, followed by an acceleration as the configuration transitions to the fuselage top, where the flow approaches free stream conditions once again. The FUN3D data shows a large suction peak as the flow accelerates around the strut-fuselage intersection on the bottom of the fuselage, which influences the pressure on the fuselage surface until the top half of the fuselage is reached. Since the strut for the Freeman and Mineck[23] test is not located or sized identically with the Mineck and Althoff-Gorton[24] strut that was modeled here, the data do not correlate with experiment, as is to be expected. This was verified by running the isolated fuselage without the strut, where it was observed that the only differences in the solution

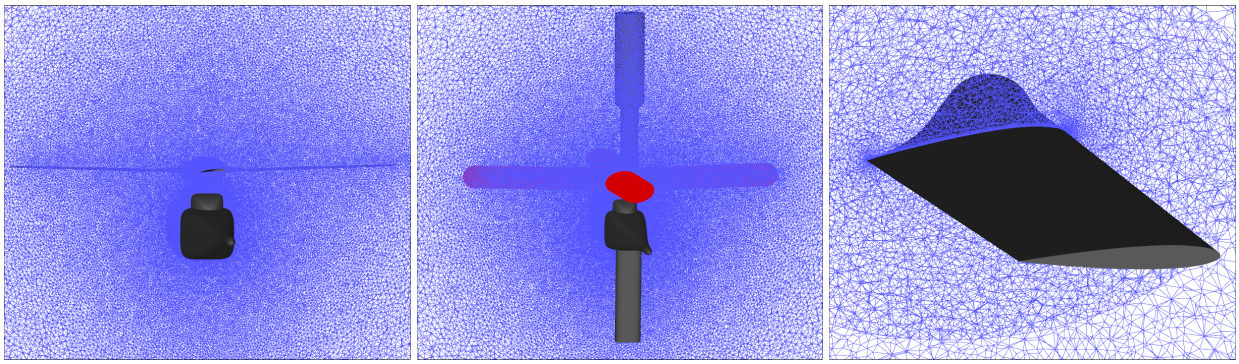

Figure 1: Robin overset grid for unstructured RANS. Left: View looking forward from wake region, Middle: Rotor grids overset in fuselage grid, including strut and rotor mount, RIght: Slice of rotor grid.

occurred at the $x/l = 1.16$ and $x/l = 1.35$ locations, documented in Fig. 4. The influence of the hub, when analyzed with FUN3D, was almost negligible, and it is not presented for that reason.

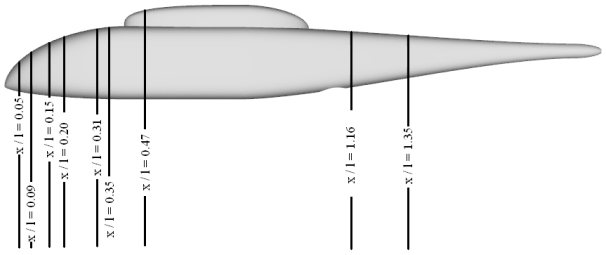

Figure 2: Experimental data locations with respect to the ROBIN fuselage model.[23]

While the data from both simulations correlate well, there are some interesting features of the analysis to note. The inviscid panel method applied for the VTM simulations typically indicates a flow acceleration from the bottom of the fuselage as it transitions to the sides, followed by pressure compressions and expansions as discussed in the prior paragraph. The viscous RANS data and the experimental data, where available, indicate a flow pattern that reflects less acceleration and deceleration from the lower to the upper fuselage. Another interesting aspect of this analysis is that the VTM inviscid simulation captured the pressures at the two farthest fuselage stations quite well without modeling the fuselage strut, which is in contrast to the viscous RANS CFD results from FUN3D. In particular at the $x/l = 1.35$ location, the fuselage radius is contracting quite rapidly, and the three-dimensional viscous flow appears to remain relatively constant along the sides of the fuselage unless the additional acceleration provided by the blockage due to the fuselage sting is included. These FUN3D results are similar to the behavior reported by Renaud *et al.*[39] on the influence of the strut during model-scale Dauphin studies.

To minimize the differences due to the modeling assumptions of the fuselage, the FUN3D simulations were therefore run with the strut and hub, although the inclusion of these components added additional computational expense.

5.2. Rotor-Fuselage Unsteady Fuselage Pressure

Subsequent to the isolated fuselage evaluation, the rotor-fuselage interactions at the flight conditions in Table 1 were computed and compared. Experimental unsteady pressure data from the Mineck and Althoff test[24] at four different centerline pressure locations were correlated with the computational results.

The control settings reported in Table 1 were applied by the VTM and FUN3D codes during their initial computations. In order to obtain data from which valid assessments could be made, these test cases were trimmed to approximate the thrust condition in the experiment. VTM permitted collective, lateral and longitudinal cyclic angles to vary, while FUN3D allowed only the collective angle to change during the trim process. The collectives reported in the experiment are $4^\circ - 5^\circ$ higher than the collectives necessary to achieve the nominal thrust coefficient for both computational methods, which have final collective angles within 1° of one another.

The data were extracted from the experimental test and the computations at different rates. The experimental data were available for every 1.5° of azimuth, while the VTM simulation saved data at 2.8° of azimuth and FUN3D at every 1° of azimuth. The unsteady pressures

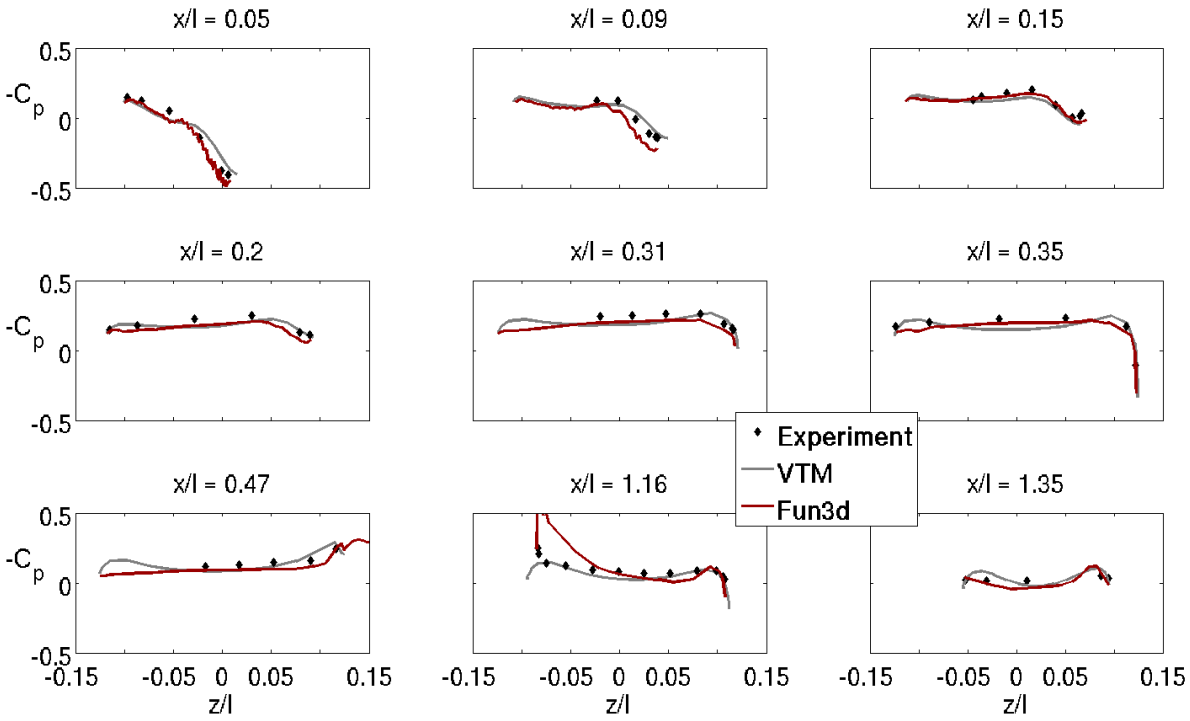

Figure 3: Isolated fuselage steady pressures for a series of fuselage stations with experimental data.[23] The VTM configuration does not model the hub and strut, while the FUN3D configuration models the hub and the strut from the Mineck and Althoff test.[24]

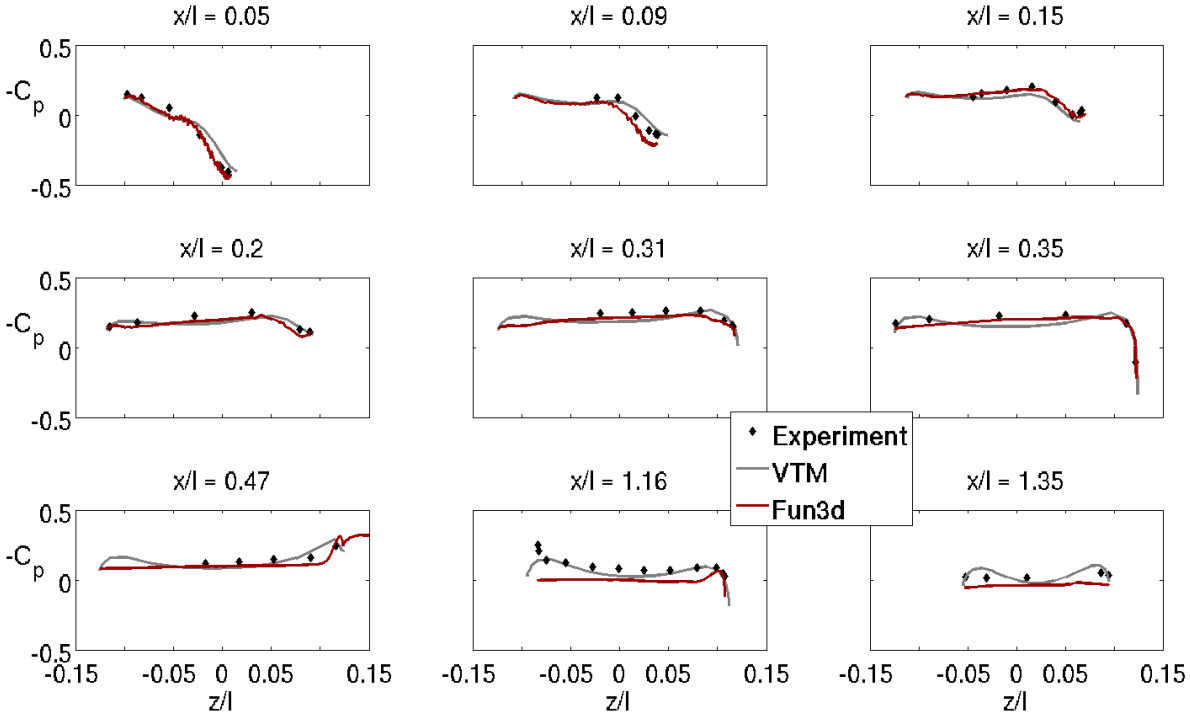

Figure 4: Isolated fuselage steady pressures for a series of fuselage stations with experimental data [23] using FUN3D and VTM configurations without hub or strut.

were extracted using the formula

$$C'_p = \frac{p - p_\infty}{0.5\rho(\Omega R)^2} \times 100 \quad (3)$$

to create a modified pressure coefficient. This modified coefficient is related to the rotor tip speed, avoiding numerical divergence as the free stream Mach number approaches zero (hover). This quantity is multiplied by 100 so that the magnitude is more amenable to plotting and analysis. The high frequency of data extraction, coupled with the small differences in $p - p_\infty$ for a mixed incompressible-compressible Mach regime resulted in FUN3D modified pressure coefficients that exhibited small oscillations about the mean behavior. These oscillations, once plotted, in many instances obscured the experimental and/or VTM data. Therefore, the data are averaged using a moving interval over a single rotor revolution in lieu of averaging the data over many revolutions, as is the case with the experimental data. The moving average analysis was evaluated using multiple ranges to ensure that the character of the time-dependent data was not compromised when the oscillations were removed.

The modified pressure coefficients (mean values removed) for the advance ratio $\mu = 0.15$ and thrust coefficient $C_T = 0.0064$ are examined in Fig. 5. For the $x/l = 0.20$ location, the computational and experimental pressures correlate very well for both phase and magnitude. For the $x/l = 0.90$ centerline location, located on the top of the fuselage doghouse, VTM results significantly deviate from the magnitude and phase of the experimental fluctuating pressures. The FUN3D phase and magnitude predictions fall between the VTM and experimental data. Similar behavior for all of the Table 1 test cases at the $x/l = 0.90$ location were observed. Kenyon and Brown[19] attribute the VTM differences to the lack of a rotor hub in VTM simulation. O'Brien and Smith have previously noted[5] that it is important in the ROBIN and similar RFI configurations to model the test components for accurate correlations with experimental data. The FUN3D simulation does model an approximate rotor hub, and its modified pressure coefficients correlate closer to the experimental behavior at this location. As the VTM and FUN3D predictions compare much more favorably at the other fuselage locations, and since FUN3D does model an approximate hub, it appears that this is indeed the cause of the differences observed at $x/l = 0.90$.

The influence of the rotor hub on the pressure differences noted at $x/l = 0.90$ are further investigated by examining the pressures at two height locations on the advancing and retreating sides of the fuselage (Fig. 6). The experimental data show clear asymmetric behavior on the advancing and retreating sides of the fuselage, in particular at $z/l = 0.08$, which is not replicated by either VTM or FUN3D. The effect of the inviscid assumption in VTM is observed in these simulations by the regular oscillatory behavior of the fluctuating pressures. The experiment and FUN3D simulations exhibit unsteadiness, in particular during the blade over pressure. The amplitude of the advancing side behavior is well-captured by the computational methods, but neither capture the larger amplitudes on the retreating side. FUN3D predicts the rate of pressure recovery after the blade passage, but not the rate of compression as the blade approaches. Higher on the fuselage at the doghouse at the $z/l = 0.13$, the experimental flow does not exhibit a strong oscillatory behavior. This is also mirrored by the FUN3D simulation, but not by the VTM results, which points to the presence of viscous effects. These FUN3D computations applied the Menter kω-SST turbulence model for turbulence closure. Lynch and Smith have observed[37] that separated, unsteady flows around bluff bodies can be more accurately predicted with a hybrid RANS-LES turbulence method. Further studies with the advanced model may be warranted to further differentiate the influence of turbulence modeling from the fidelity of the configuration used in the simulations. Examination of the FUN3D vorticity magnitude (Fig.7) at $x/l = 0.9$ shows a small asymmetry where vorticity shed from the external hub interacts with the rotor root vortices. Only a mild influence of this asymmetry is observed along the sides of the doghouse, and the asymmetry has essentially disappeared at lower locations on the fuselage body.

At the $x/l = 1.56$ fuselage station of Fig. 5, the FUN3D and VTM magnitude are comparable with experiment. At the positive peak, the VTM prediction leads the FUN3D and experimental results by about 5°, while at the negative peak, it leads by approximately 20°. Another interesting observation for this location is that the FUN3D unsteadiness reflects some of the unsteady features of the experimental data. In particular, during the downstroke of the cycle, oscillatory behavior at approximately 30°, 100°, 200°, and 290° azimuth locations is predicted by both the experimental and FUN3D simulations.

The asymmetry becomes apparent at the end of the doghouse in Fig. 8. This asymmetry remains as x/l approaches the closed tip value. Separation from the doghouse-fuselage intersection drives a portion of the asymmetry and impacts the pressures, in particular at $x/l = 1.18$. Downstream of the doghouse at $x/l = 1.56$, vorticity shed from the hub and strut becomes an important component of the flow field, as seen in Fig. 9. Vortices shed from the rotor hub at the top of the figure becomes entrained in the rotor root vorticity. As rotor blade approaches the empennage, the vorticity moves down and around the doghouse, minimizing the separated flow at the rear of the doghouse. The tip vortices

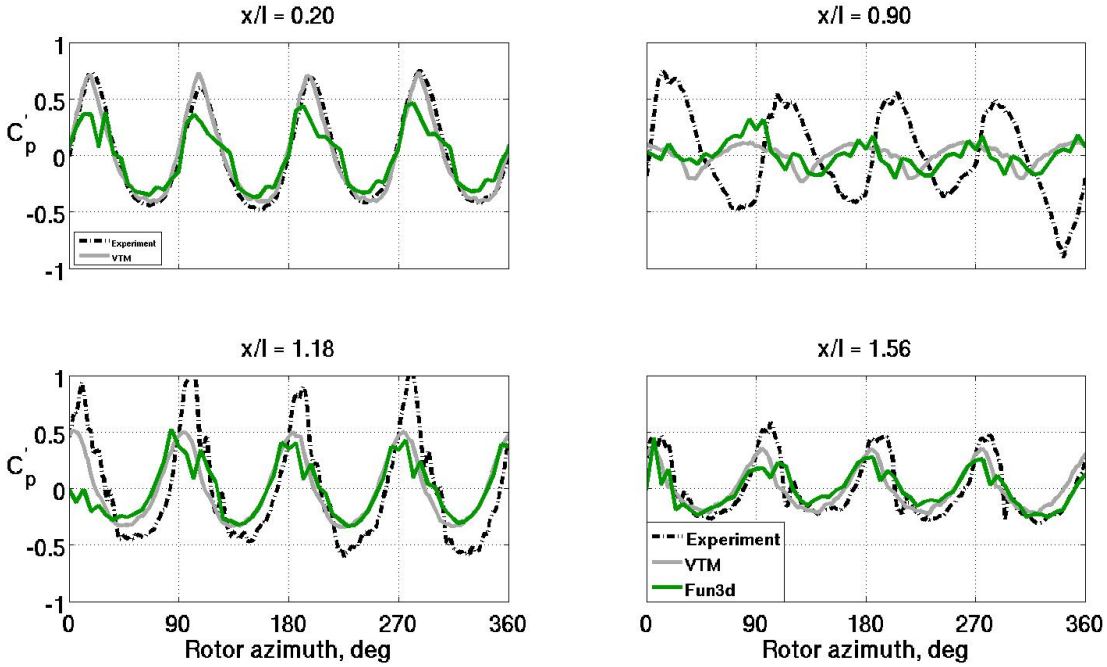

Figure 5: Variation of modified pressure coefficient with azimuth location (time) for $\mu = 0.15$ and $C_T = 0.0064$ at selected locations on the top centerline of the fuselage.

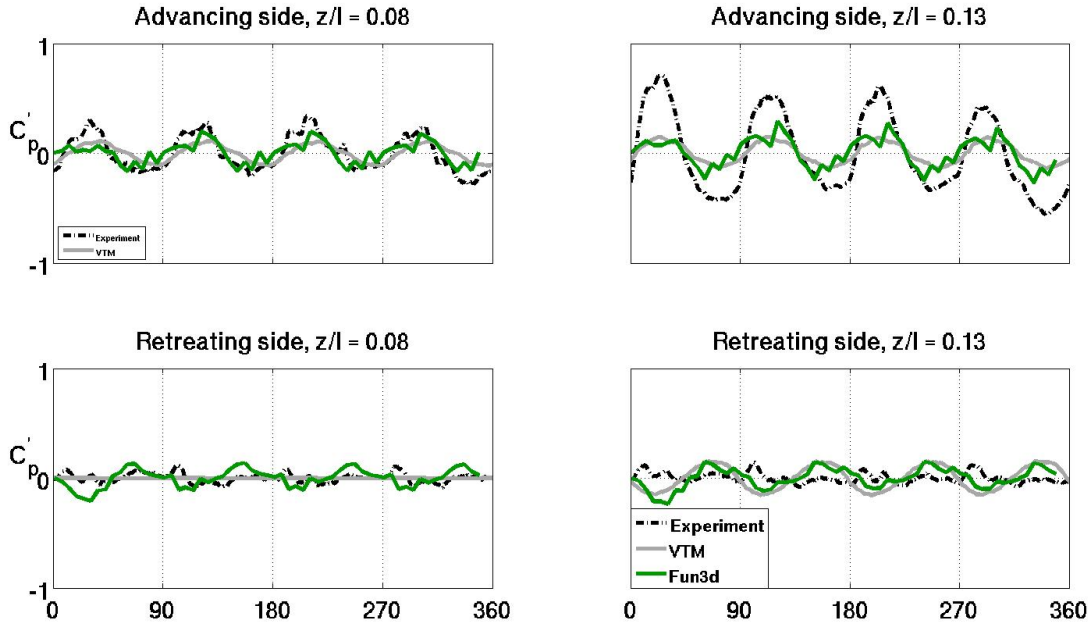

Figure 6: Variation of modified pressure coefficient with azimuth location (time) for $\mu = 0.15$ and $C_T = 0.0064$ at $x/l = 0.90$.

interact with the fuselage at the tail, and interact with the shed vorticity from the fuselage mount. A sequence typical of that observed in the higher advance ratio cases is shown in Fig. 10.

The highest advance ratio-thrust coefficient combination of $\mu = 0.23$ and $C_T = 0.0080$ exhibits similar behavior observed in the other test cases, as seen in Fig. 11. The behavior of the VTM and FUN3D simulations in the region of the doghouse previously discuss is repeated here. Aft of the doghouse at $x/l = 1.18$, experimental results have a significantly larger magnitude than the computational simulations. The FUN3D simulations show an area of flow separation that is not predicted with the VTM inviscid computations, resulting in a larger magnitude and phase shift, that is closer to the experimental predictions. This implies as before that the blade passage modifies this area of separated flow, and that a more advanced turbulence model than the Menter kω-SST RANS model may be warranted. As observed in the prior example, at $x/l = 1.56$, the VTM and FUN3D simulations are similar, although again the FUN3D solution shows a small improvement over VTM.

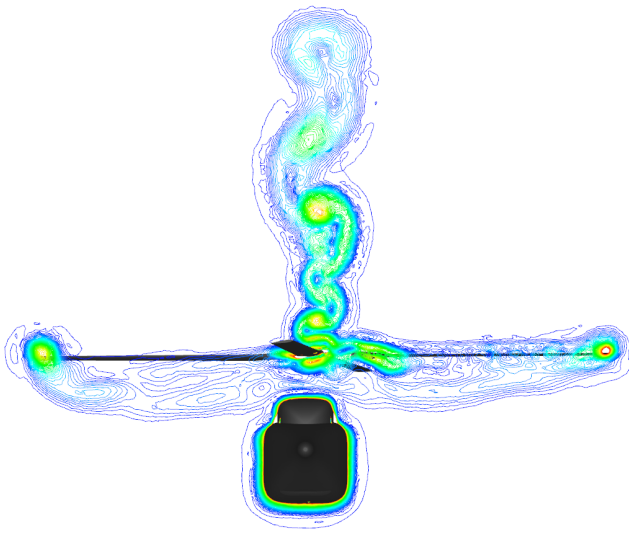

Figure 7: Vorticity magnitude at $\psi = 0^\circ$ and $x/l = 0.9$ for $\mu = 0.15$ and $C_T = 0.0064$.

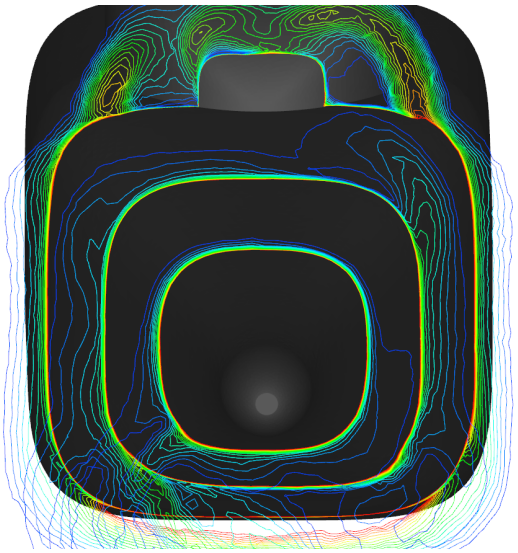

Figure 8: Vorticity magnitude at $\psi = 0^\circ$ along the empennage of the ROBIN configuration.

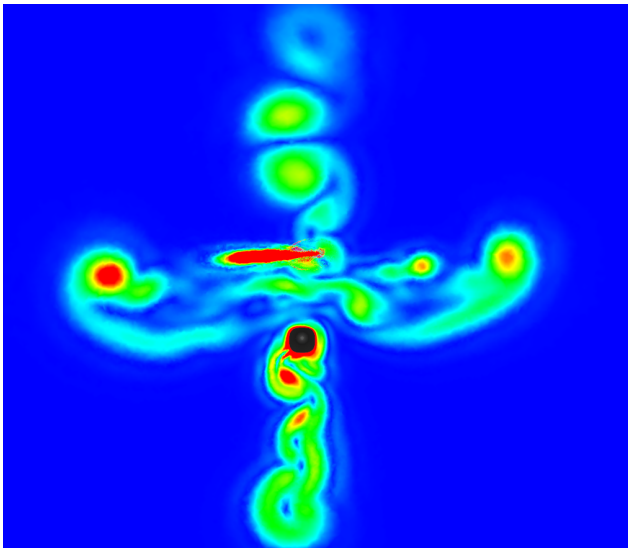

Figure 9: Vorticity magnitude at $\psi = 0^\circ$ and $x/l = 1.56$ for $\mu = 0.15$ and $C_T = 0.0064$.

The frequency content of the computational predictions can also provide some insight into the rotor-fuselage interactions. A Fast Fourier Transform (FFT) was performed for the modified pressure coefficients at the four locations compared previously. For continuity, the same two test cases are discussed here. To ensure that there was no bias introduced in the analysis, the data was sampled at every 3°, so that all methods were analyzed with the same frequency. Because the blade is rigid, and the rotor has 4 blades, the 4/rev frequencies are dominant. For simplicity, the non-dominant frequencies are omitted from the analysis. Frequency data for the two test cases used for illustrative purposes are provided in

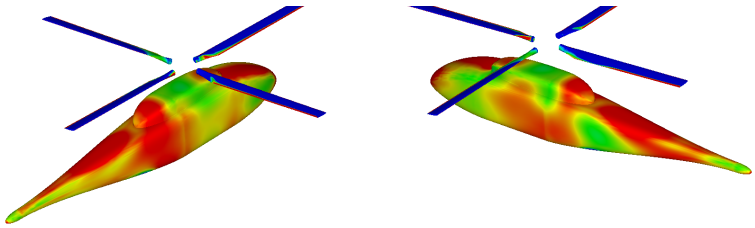

(a) $\psi = 0°$

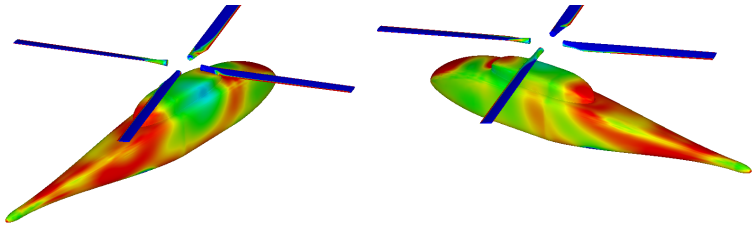

(b) $\psi = 20°$

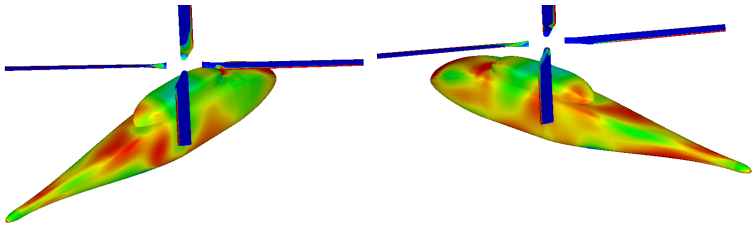

(c) $\psi = 40°$

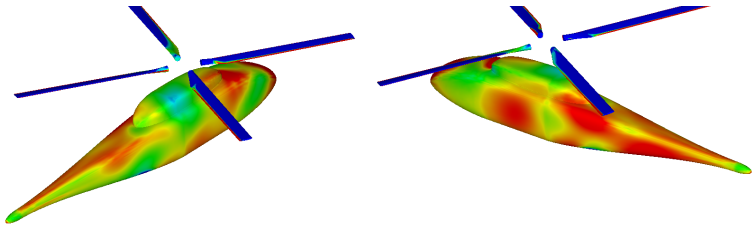

(d) $\psi = 60°$

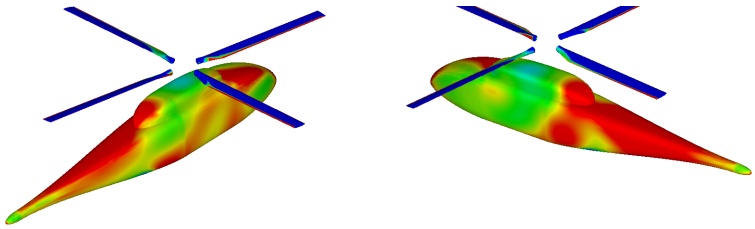

(e) $\psi = 80°$

Figure 10: Variation in the surface pressures over a quarter revolution for $\mu = 0.15$ and $C_T = 0.0064$.

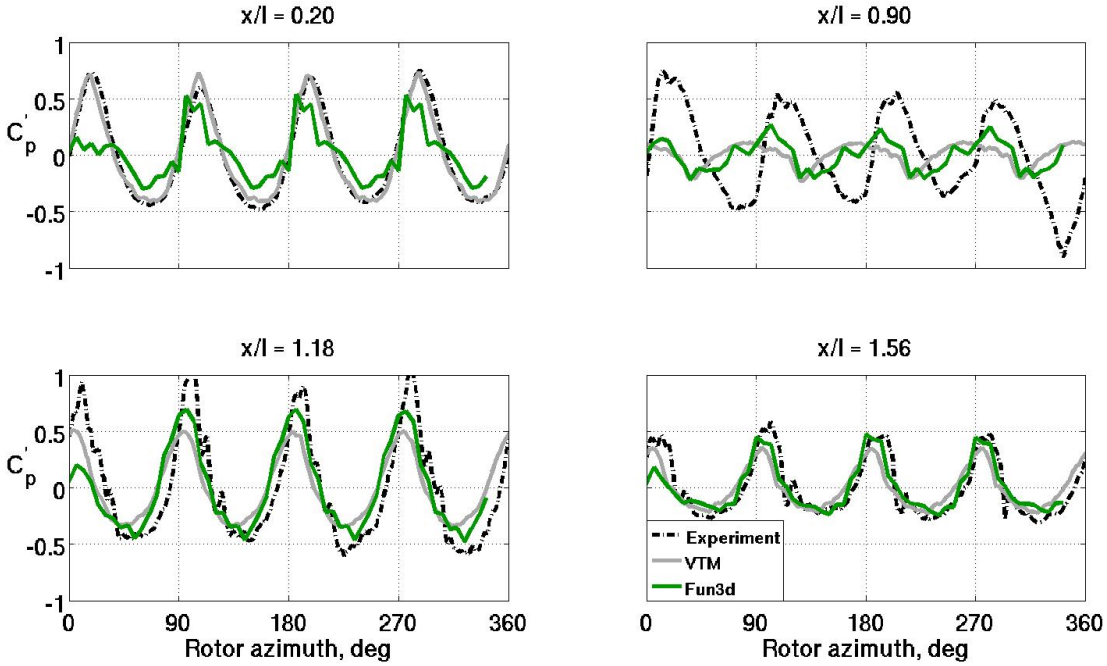

Figure 11: Variation of modified pressure coefficient with azimuth location (time) for $\mu = 0.23$ and $C_T = 0.0080$ at selected locations on the top centerline of the fuselage.

Table 3: Mineck and Althoff-Gorton[24] test cases with applicable trim.

		Experimental				VTM				FUN3D	
μ	α_s (°)	C_T	θ_0 (°)	θ_{1c} (°)	θ_{1s} (°)	C_T	θ_0 (°)	θ_{1c} (°)	θ_{1s} (°)	C_T	θ_0 (°)
0.05	0.0	0.0064	11.9	-1.3	1.3	0.0064	6.8	-2.3	1.2	0.0065	7.1
0.15	-3.0	0.0064	10.3	-2.7	2.4	0.0064	6.3	-2.3	2.1	0.0063	6.6
0.23	-3.0	0.0040	8.2	-0.5	3.8	0.0040	4.3	-1.5	2.1	0.0043	3.9
0.23	-3.0	0.0064	10.4	-0.4	3.8	0.0064	6.3	-2.1	3.3	0.0066	5.8
0.23	-3.0	0.0080	11.9	-1.3	4.0	0.0080	7.9	-2.6	4.3	0.0080	7.1

Fig. 12 and 13. From these and the other test cases, the VTM and FUN3D results are observed to generally be comparable. In cases where they are not comparable, VTM tends to predict the 4/rev frequency content slightly better than FUN3D, but the reverse is typically correct for the 8/rev and 12/rev data. No conclusions can be drawn for the 16/rev data.

5.3. Rotor-Fuselage Wake

The wake structure predicted by FUN3D is shown in Fig. 14 for three different advance ratios. At $\mu = 0.05$, the forward speed is minimal and the wake resembles that of a rotor in near-hover conditions, distorted where the empennage extends beyond the extent of the rotor radius. Increasing the advance ratio to $\mu = 0.15$ and $\mu = 0.23$ increases the skew angle of the wake, as is expected. In comparing vorticity magnitude contours from the VTM[19] and FUN3D results, the skew angles are observed to be similar. The super vortex is more pronounced in the FUN3D simulation, obscuring the details of the roll-up of the tip vortices as they merge together, which are visible in the VTM simulation.[19] The smearing of the vortex details is an artifact of the grid density and algorithm dissipation, also observed and reported in other studies.[10] Obrien has shown[3] that static feature adaptation available in FUN3D can refine the grids in the region of the tip vortex to improve the fidelity of the wake features. Top views of the wake (Fig. 15) reveal that for the locations not obscured by the super vortex, the individual tip vortices are well-captured and are similar to wake vortex structure predicted by VTM.

A more accurate assessment of the wake geometry was made using two additional test cases (Table 2) from the Ghee and Elliott[26] campaign. As with the prior investigation, the computational simulations adjusted the test controls to match the nominal thrust coefficient. Unlike the unsteady pressure simulations cases, the experimental collective angles proved to be good estimates of the computational collective angles to achieve the nominal thrust coefficient 4.

Smoke visualizations of longitudinal slices of the flow field at $y/R = \pm 0.3$ and $y/R = \pm 0.8$ locations are available from the ROBIN experiment. At these locations, the vorticity predicted by the numerical simulations was extracted and compared to the experimental data in Figs. 16 and 17. The vertical location of the FUN3D and VTM vorticity indicate that the wake geometries predicted by the numerical methods are very similar, in spite of the diffused super vortex observed in the FUN3D simulation. The initial upwash on the outer advancing side of the rotor is generally captured by the FUN3D simuiation. The wake trajectories were compared only for a downstream x/l distance equivalent to the fuselage length, as the FUN3d simulations were not computed to long wake ages.

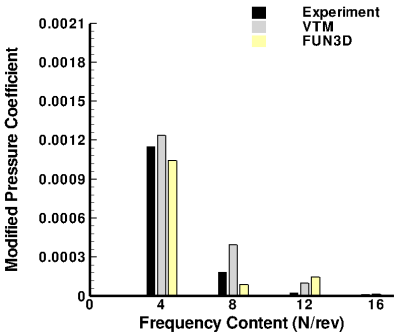

(a) $x/l = 0.20$

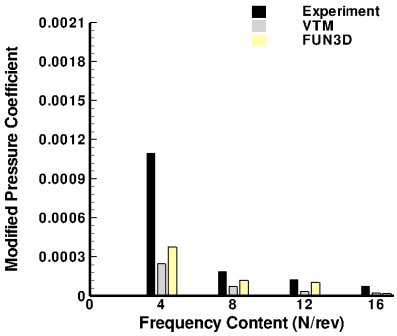

(b) $x/l = 0.90$

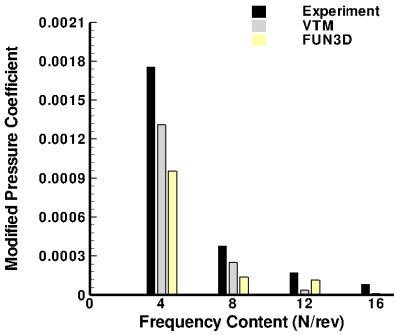

(c) $x/l = 1.18$

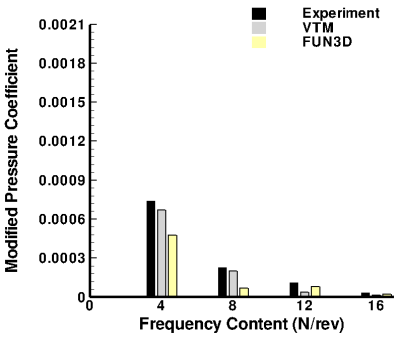

(d) $x/l = 1.56$

Figure 12: Frequency content of the center line modified surface pressure for $\mu = 0.15$ and $C_T = 0.0064$.

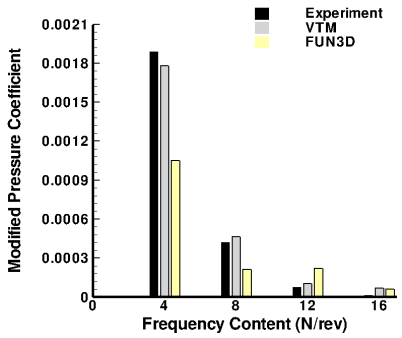

(a) $x/l = 0.20$

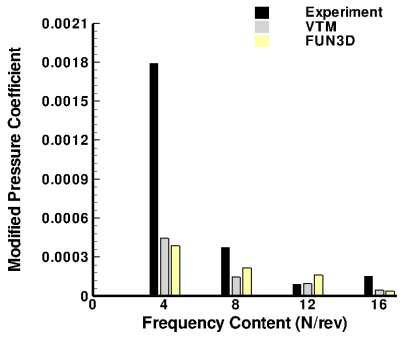

(b) $x/l = 0.90$

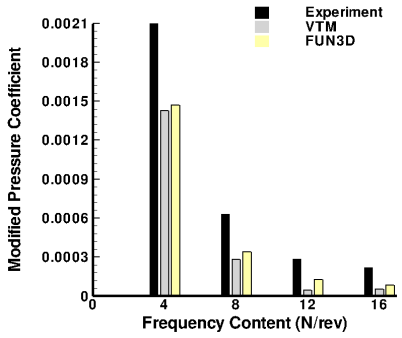

(c) $x/l = 1.18$

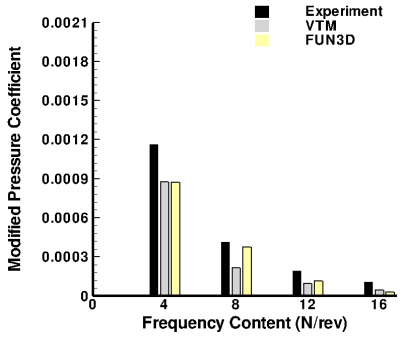

(d) $x/l = 1.56$

Figure 13: Frequency content of the center line modified surface pressure for $\mu = 0.23$ and $C_T = 0.0080$.

6. CONCLUSIONS

The vortex transport method (VTM) has been compared with an unstructured Reynolds-averaged Navier-Stokes (RANS) method for rotor-fuselage interaction using the ROBIN configuration. Steady and unsteady pressure solutions and wake trajectories have been correlated with experimental data. Some conclusions can be drawn from the basis of this work:

1. FUN3D and VTM (coupled with an inviscid panel method) provide comparable instantaneous and time-averaged fuselage pressures for the rotor-fuselage interaction. FUN3D solutions are slightly more accurate for higher advance ratios, indicating that the unsteady low Mach preconditioning may help to resolve mixed flows at the near-hover flight conditions when the incompressible path cannot be applied due to compressible tip Mach numbers.
2. Wake features, such as the tip vortices over longer wake ages, are more sharply defined by VTM compared with a moderate size FUN3D grid. Prior work has shown that the rotor wake features can be sharpened in FUN3D if grid adaptation or refinement is applied.
3. The frequency content of the surface pressures predicted by VTM and FUN3D are fairly comparable. In instances where the predictions are not comparable, VTM tends predict the 4/rev values slightly better, while FUN3D is slightly more accurate for the 8/rev and 12/rev data.
4. Test features such as rotor hubs and fuselage struts can influence asymmetric fuselage surface pressures near or downstream of these components. These include both steady pressures and unsteady pressure fluctuations.
5. The character of the unsteadiness (above 4/rev) of the experimental surface pressure data observed at some locations appears to be caused by viscous-dominated interactions such as separation. Excellent correlations of VTM, FUN3D and experiment where these effects are not dominant suggests that if a viscous solver is coupled with VTM, these effects will be captured.
6. The wake skew angles and lateral locations for VTM and FUN3D correlate overall very well; the FUN3D skew angles are more easily discerned for the inboard locations of the rotor.

7. ACKNOWLEDGMENTS

The Georgia Tech portion of this effort was sponsored in part by the Vertical Lift Center of Excellence at the

Table 4: Ghee and Elliott[26] wake visualization test cases with applicable trim.

		Experimental					VTM					FUN3D	
μ	α_s (°)	C_T	β_0 (°)	θ_0 (°)	θ_{1c} (°)	θ_{1s} (°)	C_T	β_0 (°)	θ_0 (°)	θ_{1c} (°)	θ_{1s} (°)	C_T	θ_0 (°)
0.15	-3.0	0.0064	1.5	6.6	-1.4	2.0	0.0063	1.7	6.2	-2.3	2.1	0.0062	6.4
0.23	-3.0	0.0064	1.5	6.5	-1.1	3.2	0.0064	1.7	6.3	-2.2	3.4	0.0063	5.9

Georgia Institute of Technology. Dr. Michael Rutkowski has been the technical monitor of this center. Computational support was provided through the DoD High Performance Computing Centers at NAVO through an HPC grant from the US Army. Dr. Roger Strawn is the S/AAA of this grant. The computer resources of the Department of Defense Major Shared Resource Centers (MSRC) are gratefully acknowledged. The authors would like to thank Mr. Nicholas Liggett, and especially Mr. Phillip Richards at Georgia Tech for their aid in post-processing the FUN3D data.

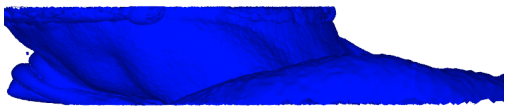

(a) $\mu = 0.05$

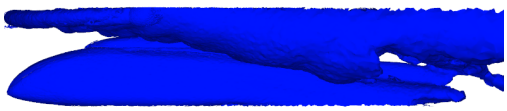

(b) $\mu = 0.15$

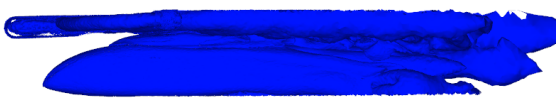

(c) $\mu = 0.23$

Figure 14: Side views of the rotor wakes for various advance ratios at a $C_T = 0.0064$.

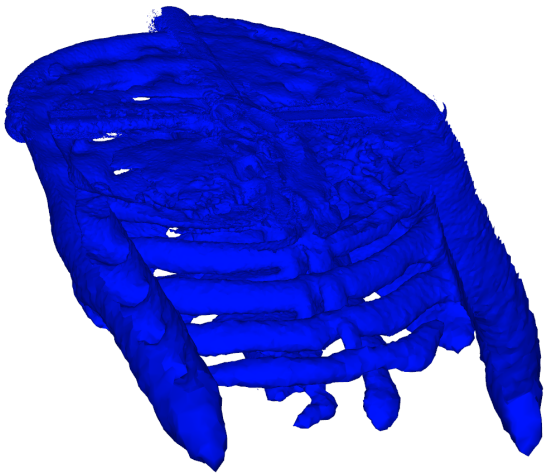

(a) $\mu = 0.15$

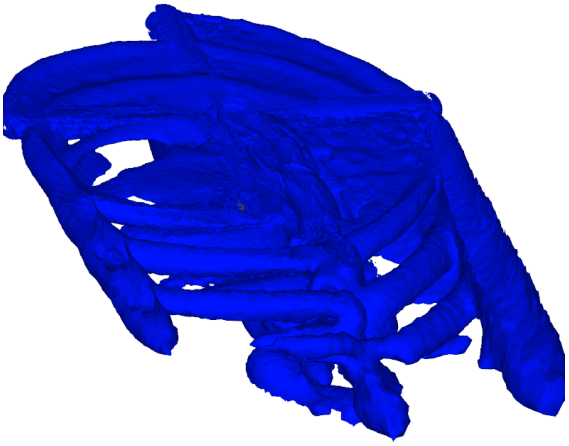

(b) $\mu = 0.23$

Figure 15: Top views of the rotor wakes for various advance ratios at a $C_T = 0.0064$.

References

[1] Strawn, R., Caradonna, F., and Duque, E., "30 Years of Rotorcraft Computational Fluid Dynamics Research and Development," *Journal of the Ameri-*

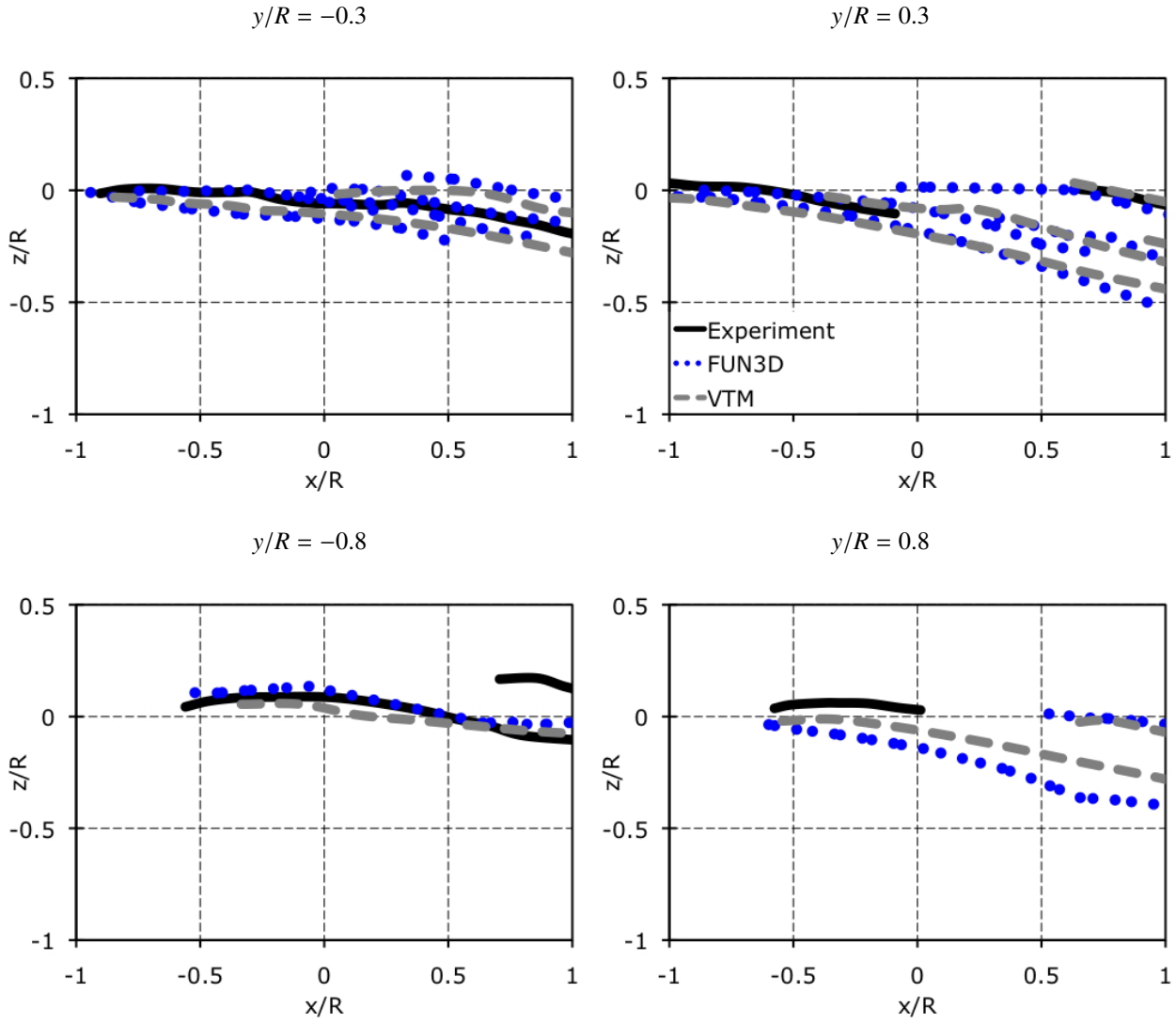

Figure 16: Sideline vortex trajectories for $\mu = 0.15$ and $C_T = 0.0064$.

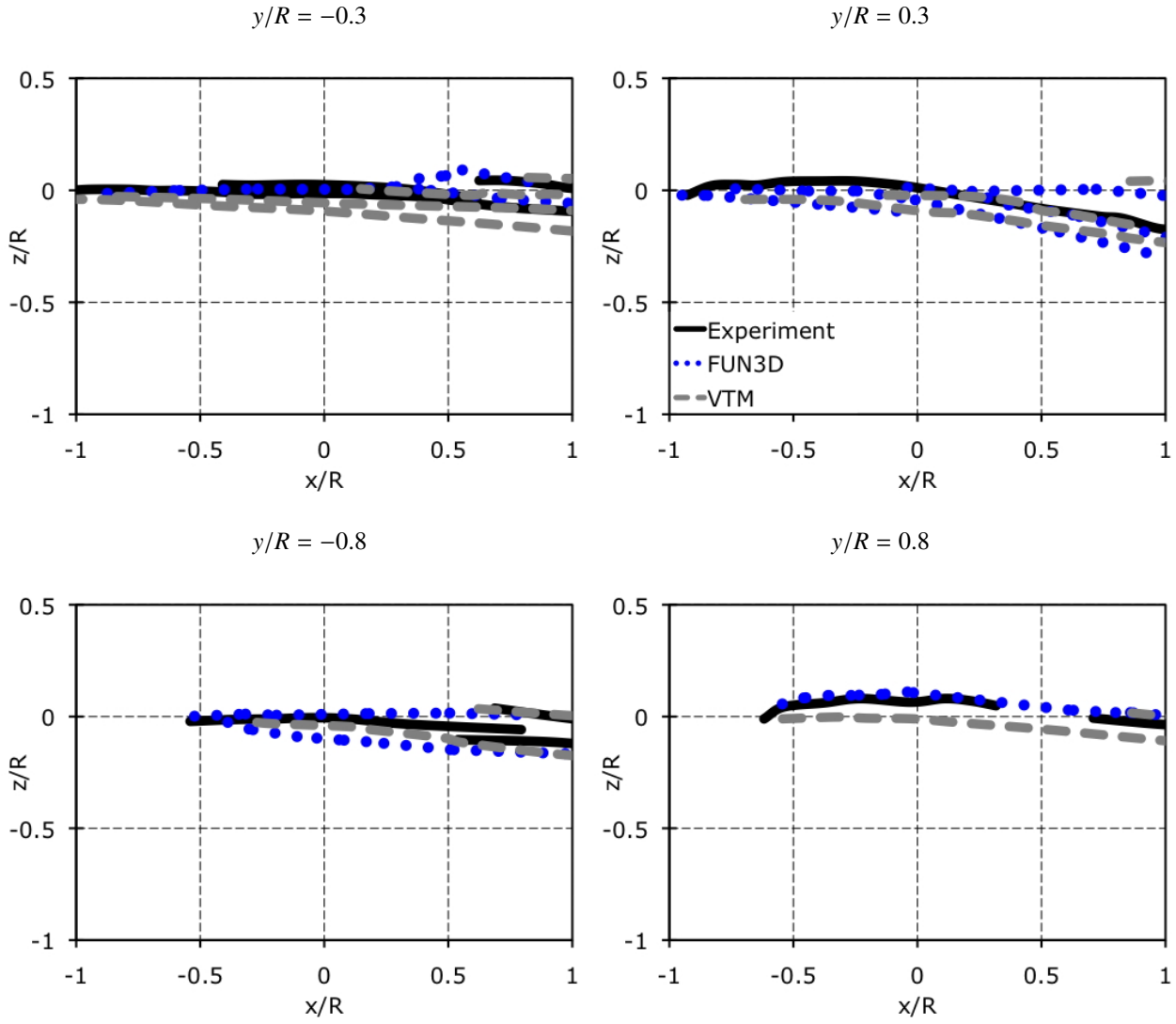

Figure 17: Sideline vortex trajectories for $\mu = 0.23$ and $C_T = 0.0064$.

can Helicopter Society, Vol. 51, No. 1, 2006, pp. 5–21.

[2] Strawn, R. and Djomehri, M., "Computational Modeling of Hovering Rotor and Wake Aerodynamics," *Journal of Aircraft*, Vol. 39, No. 5, 2002, pp. 786–793.

[3] O'Brien Jr, D., *Analysis Of Computational Modeling Techniques For Complete Rotorcraft Configurations*, Ph.D. thesis, Georgia Institute of Technology, May 2006.

[4] Potsdam, M. and Strawn, R., "CFD Simulations of Tiltrotor Configurations in Hover," *Proceedings of the American Helicopter Society Annual Forum*, Vol. 58, 2002, pp. 681–696.

[5] O'Brien, D. and Smith, M., "Understanding the Physical Implications of Approximate Rotor Methods Using an Unstructured CFD Method," *Proceedings of the* 31^{st} *European Rotorcraft Forum, Florence, Italy*, September 2005.

[6] Ruffin, S., O'Brien, D., Smith, M., Hariharan, N., Lee, J., and Sankar, L., "Comparison of Rotor-Airframe Interaction Utilizing Overset and Unstructured Grid Techniques," 42^{nd} *AIAA Aerospace Sciences Meeting and Exhibit*, Vol. 46, January 2004.

[7] Sitaraman, J., Katz, A., Jayaraman, B., Wissink, A., and Sankaran, V., "Evaluation of a Multi-Solver Paradigm for CFD using Unstructured and Structured Adaptive Cartesian Grids," AIAA-2008-0660, 46 th AIAA Aerosciences Conference, Reno NV, 2008.

[8] Lee, J. and Kwon, O., "Predicting Aerodynamic Rotor-Fuselage Interactions by Using Unstructured Meshes," *Transactions of the Japan Soceity for Aeronautical and Space Sciences*, Vol. 44, No. 146, 2005, pp. 208–216.

[9] Steijl, R. and Barakos, G., "Sliding Mesh Algorithm for CFD Analysis of Helicopter Rotor-Fuselage Aerodynamics," *International Journal for Numerical Methods in Fluids*, Vol. 58, No. 5, 2008.

[10] Potsdam, M., Smith, M. J., and Renaud, T., "Unsteady Computations of Rotor-Fuselage Interaction," *Proceedings of the* 35^{th} *European Rotorcraft Forum, Hamburg, Germany*, September 2009.

[11] Komerath, N. and Smith, M., "Rotorcraft Wake Modeling: Past, Present and Future," 35^{th} European Rotorcraft Forum, Hamburg, Germany, September 2009.

[12] Brown, R., "Rotor Wake Modeling for Flight Dynamic Simulation of Helicopters," *AIAA Journal*, Vol. 38, No. 1, 2000, pp. 57–63.

[13] Brown, R. and Line, A., "Efficient High-Resolution Wake Modeling Using the Vorticity Transport Equation," *AIAA Journal*, Vol. 43, No. 7, 2005, pp. 1434.

[14] Brown, R. and Houston, S., "Comparison of Induced Velocity Models for Helicopter Flight Mechanics," *Journal of Aircraft*, Vol. 37, No. 4, 2000, pp. 623–629.

[15] Houston, S. and Brown, R., "Rotor-Wake Modeling for Simulation of Helicopter Flight Mechanics in Autorotation," *Journal of Aircraft*, Vol. 40, No. 5, 2003, pp. 938–945.

[16] Whitehouse, G. R. and Brown, R. E., "Modeling the Mutual Distortions of Interacting Helicopter and Aircraft Wakes," *Journal of Aircraft*.

[17] Ahlin, G. and Brown, R., "The Vortex Dynamics of the Rotor Vortex Ring Phenomenon," *Proceedings of the American Helicopter Society* 63^{rd} *Annual Forum*, 2007.

[18] Phillips, C. and Brown, R., "Eulerian Simulation of the Fluid Dynamics of Helicopter Brownout," *American Helicopter Society* 64^{th} *Annual Forum Proceedings, Montréal, Canada*, 2008.

[19] Kenyon, A. and Brown, R., "Wake Dynamics and Rotor-Fuselage Aerodynamic Interactions," *Journal of the American Helicopter Society*, Vol. 54, No. 1, 2009.

[20] Kelly, M., Duraisamy, K., and Brown, R., "Predicting Blade Vortex Interaction, Airloads and Acoustics Using the Vorticity Transport Model," January 2008.

[21] Fletcher, T. and Brown, R., "Main Rotor-Tail Rotor Wake Interaction and its Implications for Helicopter Directional Control," 32^{nd} *European Rotorcraft Forum*, September 2009.

[22] Kim, H., Kenyon, A., Duraisamy, K., and Brown, R., "Interactional Aerodynamics and Acoustics of a Hingeless Coaxial Helicopter with an Auxiliary Propeller in Forward Flight," 2008.

[23] Freeman, C. and Mineck, R., "Fuselage surface pressure measurements of a helicopter wind-tunnel model with a 3. 15-meter diameter single rotor," Tech. rep., 1979.

[24] Mineck, R. and Gorton, S., "Steady and periodic pressure measurements on a generic helicopter fuselage model in the presence of a rotor," 2000.

[25] Boyd, D., 2006, private communication with Prof. R. Brown.

[26] Ghee, T. A. and Elliott, J. W., "The Wake of a Small-Scale Rotor in Forward Flight Using Flow Visualization," *Journal of the American Helicopter Society*, Vol. 40, No. 3, 1995, pp. 52 – 65.

[27] Bonhaus, D., *An upwind multigrid method for solving viscous flows on unstructured triangular meshes*, Ph.D. thesis, Citeseer, 1993.

[28] Anderson, W., Rausch, R., and Bonhaus, D., "Implicit/multigrid algorithms for incompressible turbulent flows on unstructured grids," *Journal of Computational Physics*, Vol. 128, No. 2, 1996, pp. 391–408.

[29] Abras, J., *Enhancement of Aeroelastic Rotor Airload Prediction Methods*, Ph.D. thesis, Georgia Institute of Technology, April 2009.

[30] Nielsen, E., Hampton, V., Lee-Rausch, E., Lee, E., and Jones, W., "Adjoint-Based Design of Rotors Using the Navier-Stokes Equations in a Noninertial Reference Frame," 2009.

[31] Lee-Rausch, E. M. and Biedron, R. T., "Simulation of an Isolated Tiltrotor in Hover with an Unstructured Overset-Grid RANS Solver," 2009.

[32] Chorin, A., "A numerical method for solving incompressible viscous flow problems," *Journal of Computational Physics*, Vol. 135, No. 2, 1997, pp. 118–125.

[33] Roe, P., "Approximate Riemann solvers, parameter vectors, and difference schemes," *Journal of computational physics*, Vol. 135, No. 2, 1997, pp. 250–258.

[34] Spalart, P. and Allmaras, S., "A one-equation turbulence model for aerodynamic flows," *AIAA, Aerospace Sciences Meeting and Exhibit, 30 th, Reno, NV*, 1992, p. 1992.

[35] Menter, F., "Two-equation eddy-viscosity turbulence models for engineering applications," *AIAA journal*, Vol. 32, No. 8, 1994, pp. 1598–1605.

[36] Spalart, P., Jou, W., Strelets, M., and Allmaras, S., "Comments on the feasibility of LES for wings, and on a hybrid RANS/LES approach," *Advances in DNS/LES*, Vol. 1, 1997.

[37] Lynch, C. and Smith, M., "Hybrid RANS-LES Turbulence Models on Unstructured Grids," No. AIAA–08–3854, 2008.

[38] Pirzadeh, S., "Three-Dimensional Unstructured Viscous Grids by the Advancing Layers Method," *AIAA Journal*, Vol. 34, No. 1, 1996, pp. 43–49.

[39] Renaud, T., O'Brien, D., Smith, M., and Potsdam, M., "Evaluation of Isolated Fuselage and Rotor-Fuselage Interaction using CFD," *Journal of the American Helicopter Society*, Vol. 53, No. 1, 2008, pp. 3 – 17.